Latest results on searching for fractionally charged particles with the DAMPE experiment

Chengming Liu,[a,b,*] Yifeng Wei[a,b] and Guangshun Huang[a,b] for the DAMPE collaboration

[a]State Key Laboratory of Particle Detection and Electronics, University of Science and Technology of China, Hefei 230026, China,

[b]Department of Modern Physics, University of Science and Technology of China, Hefei 230026, China

E-mail: chm6@mail.ustc.edu.cn, weiyf@ustc.edu.cn, hgs@ustc.edu.cn

The existence of fractionally charged particles (FCP) is foreseen in extensions of or beyond the Standard Model of particle physics. Most of the previously conducted searches for FCPs in cosmic rays were based on experiments underground or at high altitudes. However, there have been few searches for FCPs in cosmic rays carried out in orbit other than AMS-01 flown by a space shuttle and BESS by a balloon at the top of the atmosphere. In this study, we conduct an FCP search in space based on on-orbit data obtained using the Dark Matter Particle Explorer (DAMPE) satellite over a period of five years. Unlike underground experiments, which require an FCP energy of the order of hundreds of GeV, our FCP search starts at only a few GeV. An upper limit of 6.2×10^{-10} cm^{-2}sr^{-1}s^{-1} is obtained for the flux. Our results demonstrate that DAMPE exhibits higher sensitivity than experiments of similar types by three orders of magnitude that more stringently restricts the conditions for the existence of FCP in primary cosmic rays.

38th International Cosmic Ray Conference (ICRC2023)
26 July - 3 August, 2023
Nagoya, Japan

*Speaker

https://pos.sissa.it/

1. Introduction

In early 19th century, the Millikan Oil's drop experiment showed that all charged particles have multiples charge of electron charge [1]. Then the Quark Model by Gell-Mann and Zweig [2, 3] proposed in 1964 that quarks, as elementary particles, carry fractional charge values ($\frac{1}{3}e$ or $\frac{2}{3}e$). With the help of accelerators, many searches for free quarks have been studied. But due to the color confinement of QCD theory, quarks will not exist freely. The current research in this field looks for any free fractional charge particles.

The FCP is generally assumed as heavy lepton which will interact with materials through ionization and without hadronic or electromagnetic process. As a result, the minimum ionized particles (MIPs) is a possible feature of FCP. There are three possible sources of FCP in cosmic rays as Figure 1 shows [4]: **First**, it may be produced at the early Universe after the Big Bang and remains in some bulk matter. **Second**, it may be produced through high-energy astrophysical processes. **Third**, it may be produced in the extensive air shower of cosmic-rays.
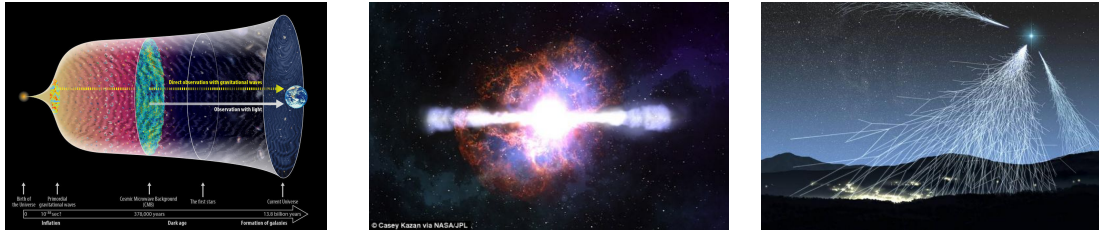
Figure 1: The possible sources of FCP in cosmic rays. From left to right, the figures illustrate the sources of early universe, celestial activities, and extensive air shower.

Table 1: The results from some typical experiments

	Experiments	Upper limit ($cm^{-2}sr^{-1}s^{-1}$)
Underground	LSD	2.7×10^{-13}
	Kamiokande II	2.1×10^{-15}
	MACRO	6.0×10^{-16}
In-space	AMS01	3.0×10^{-10}
	BESS	4.5×10^{-10}

Table 1 shows the results of some typical experiments for searching FCP from CRs [4]. Underground experiments [5–10] evade background noise from extensive air showers and attempt to observe FCPs that pass through the overburden. Such FCPs would have to start out with an energy larger than hundreds of GeV to penetrate rocks before entering the underground laboratory. With a large acceptance and long exposure time, the underground experiment MACRO obtained a flux upper limit of 6.1×10^{-16} cm^{-2}sr^{-1}s^{-1} at the 90% confidence level (C. L.) [8] for particles with charges from $\frac{1}{4}e$ to $\frac{2}{3}e$.

Searches for FCPs in cosmic rays are also conducted in space, notably, on the space shuttle (AMS-01 [11]) and balloon (BESS [12]). Compared to underground experiments, particles with significantly lower energy in the order of a few GeV are able to be observed in space experiments

where the stricter flux upper limit of 3.0×10^{-7} cm^{-2}sr^{-1}s^{-1} for FCPs was obtained from AMS-01. The DArk Matter Particle Explorer (DAMPE) has relatively larger acceptance and has been working well in space for more than seven years and as today a large amount of scientific data has been acquired. It can help to find FCP from CRs as an on-orbit experiment.

2. DAMPE mission
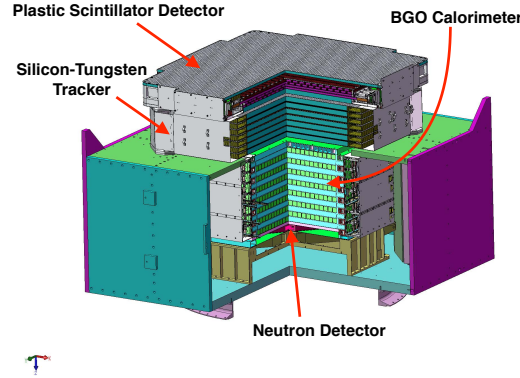
Figure 2: The structure of the DAMPE detector.

The DArk Matter Particle Explorer (DAMPE [13], also known as "Wukong" in Chinese) is an on-orbit calorimetric-type, satellite-borne detector that can be used to search for FCPs in primary cosmic rays in space. From top to bottom, DAMPE consists of four sub-detectors as shown in Fig. 2. A Plastic Scintillator Detector (PSD) [14], a Silicon-Tungsten tracKer converter (STK) [15], a Bismuth Germanium Oxide (BGO) imaging calorimeter [16], and a NeUtron Detector (NUD) [17]. The PSD and STK measure the charge of the incident particle. The BGO calorimeter measures the energy of incident particle, and provides the trigger for the DAMPE spectrometer.

DAMPE has good charge resolutions of $0.06e$ and $0.04e$ for measuring singly charged particles with the PSD [18] and STK [19], respectively. Furthermore, compared to similar types of space experiments, DAMPE has a relatively large acceptance and long exposure duration, which are advantageous in searching for FCPs. Here we conduct a search for FCPs based on on-orbit data collected with DAMPE over a period of five years. The full analysis is described in the reference [20].

3. Data analysis

3.1 Target FCPs

The on-orbit data corresponding to the latitude region of [-20°, +20°] is used to search for FCPs, where the strength of geomagnetic field is generally uniform, and the energy cutoff is usually ~ 10 GeV for singly charged particles. Given that the acceleration mechanism of cosmic rays may be related to their charge [21], FCPs carry proportionately lower energy. Combined with the heavy lepton assumption, the search for FCPs is constrained to Minimum Ionizing Particles(MIPs). The measurement of energy deposition is expressed in units of the energy deposited by a singly charged

MIP event, which deposits approximately 23 MeV in one BGO crystal [16]. The trigger system is generated by the BGO calorimeter, whose threshold for a MIP event is calibrated to be approximately $\frac{1}{5}$ MIP [22] based on on-orbit data. Thus, due to the very low trigger efficiency for FCPs with $\frac{1}{3}e$ ($\frac{1}{9}$ MIP), this study focuses on $\frac{2}{3}e$ FCPs.

3.2 Background estimation

Due to the limited charge resolution, high-energy protons/antiprotons, electrons/positrons, and high energy gamma rays are the primary sources of background noise. The BGO calorimeter is approximately 32 radiation lengths deep, thus excluding misidentifications caused by electrons/positrons and gamma rays. Moreover, the 1.6 nuclear interaction lengths deep such that 80% of protons/antiprotons develop hadronic showers; therefore, misidentification from the 20% non-showering, MIP-like high-energy protons/antiprotons is the largest source of background.

3.3 Monte Carlo simulations

Monte Carlo (MC) simulations of protons and FCPs with $\frac{2}{3}e$ based on the GEANT4 [23] are used to study the background and signals. GEANT4 is capable of performing simulations on (virtual) particles with selected mass, charge, and physical process. Thus, we insert a virtual MIP-like FCP with $\frac{2}{3}e$ within the GEANT4 framework in the DAMPE software. The processes of multiple scattering and ionization are added. The sample of MC FCPs is used as the signal to be analyzed. Both primary and secondary protons are taken into account in evaluating the background.

3.4 Event selections
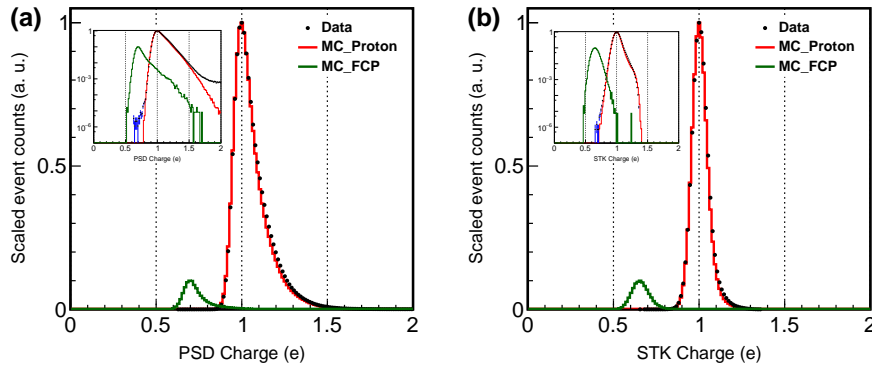
Figure 3: The distributions of charges measured by the PSD (a) and STK (b). The log scale distributions for the PSD and STK are shown in the insets [20].

The MIP events are selected during the search for FCPs. The detailed event selection method is described below.

☐ **Fiducial cut**: MIPs Trigger (MIPT) events, geometry angle, and event energy.

☐ **Track selection**: A good track should be reconstructed by the STK. The large-angle scattered events are removed.

☐ **MIPs selections**: Constrain the fired cells in PSD and BGO detectors. Require the track going through the PSD strips. Require the event penetrate the whole BGO calorimeter.

☐ **Charge reconstruction**: The PSD and STK can reconstruct charges of incident events.

The average value of two PSD layers is taken to be the PSD charge. The STK charge is also taken to be the average of the charge values corresponding to multiple layers after correction [19]. The results of charge reconstruction are depicted in Fig. 3. The charge spectra obtained from the on-orbit data (black dots) and MC protons (red line) display close similarity. MC FCPs (green line) and singly charged MIPs are adequately distinguishable in both the PSD and STK.

3.5 Definition of the signal region
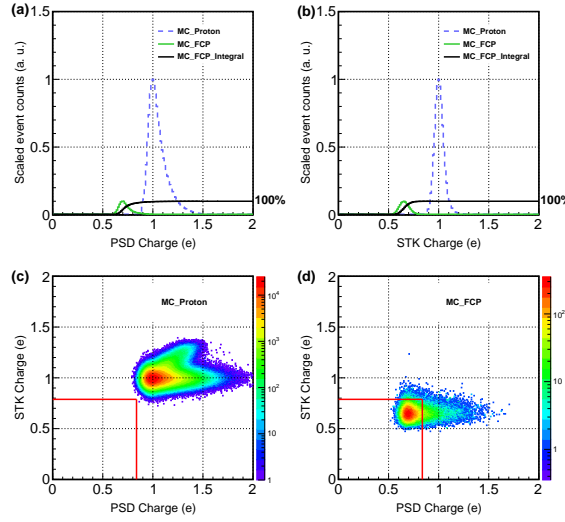
Figure 4: The charge distributions from the PSD and STK and the definition of the signal region [20]. The charge distributions for the PSD and STK are shown in panels (a) and (b), respectively. The event counts are scaled to arbitrary units. The solid green lines correspond to MC FCPs and the dashed blue lines are for MC protons. All background proton MIP events fall outside the region, as depicted in panel (c). The combined efficiency of the signal region for FCPs is approximately 86.0%, as depicted in panel (d).

The differences in the charge distributions between MC protons and MC FCPs are depicted in Fig. 4(a) and 4(b). The integrals of MC FCPs are also drawn in the corresponding panel to evaluate the selection of the signal region. The signal region is defined as the area where the charge values of the PSD and STK are less than $0.84e$ and $0.79e$, respectively. The standard deviation σ is obtained by dividing the full width at half maximum of the distributions by 2.35. The values corresponding to the signal region are obtained by adding 3σ to the peak value. The two-dimensional distributions of the PSD-STK charges of MC samples are depicted in Fig. 4(c) and 4(d) accompanied by the signal region indicated by red lines. A combined integral efficiency of the signal region of up to 86% is observed for MC FCPs, as shown in Fig. 4(d). The signal region is deemed to be adequate for excluding the background from proton MIP events, as depicted in Fig. 4(c).

Figure 5 shows the two-dimensional PSD-STK charge distribution of the on-orbit data, as well as the signal region that is shown as the red lines.
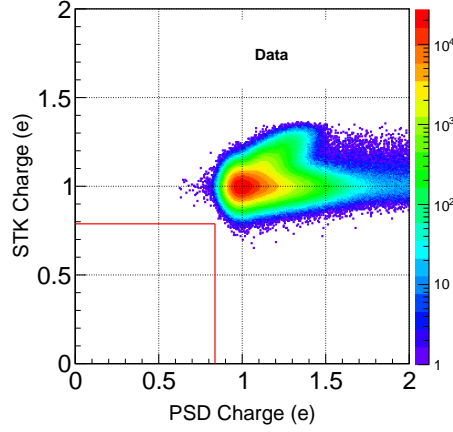
Figure 5: The distribution of PSD-STK charge for on-orbit data [20]. The red lines indicate the signal region for FCPs. The signal region is defined to cover candidate FCP event, while rejecting the proton background. No candidate event is observed to lie within the signal region. The portion above 1.1e of both PSD and STK charges corresponds to the events that inject from the bottom to the top of DAMPE. These events are low-energy secondary particles of extensive air showers.

4. Results

The flux of $\frac{2}{3}e$ FCPs is given by Eq. 1

$$\Phi = \frac{N_{obs}}{T_{exp}\epsilon_{scale}\epsilon_{trig}A_{eff}\epsilon_{region}},\qquad(1)$$

where T_{exp} denotes the effective exposure time for this work, ϵ_{scale} the pre-scale factor of MIPT, ϵ_{trig} the efficiency of the MIPT for FCPs, A_{eff} the effective acceptance for FCPs, ϵ_{region} the efficiency of the signal region for FCPs, and N_{obs} the number of observed FCPs candidates. The results reported in this work are based on data recorded from 01.01.2016 to 12.31.2020. The T_{exp} is equal to approximately 2.34×10^7 s. The MIPT pattern is used in this analysis, $\epsilon_{scale} = \frac{1}{4}$ is designed for MIPT and $\epsilon_{trig} = 85.5\%$ is based on FCP simulations. $A_{eff} = 940$ cm^{2}sr is observed following the selection process. ϵ_{region} represents the efficiency of the signal region for FCPs and is evaluated to be 86%. Since no candidate event is observed within the signal region and the amount of background is negligible, for the upper limit, N_{obs} is taken to be 2.44 at the 90% C. L. [24].

We assume that the systematic uncertainties of FCPs are the same as those of singly charged MIP events. The total systematic uncertainty of the selections is given by

$$\delta = \sqrt{\delta_{trigger}^2 + \delta_{track}^2 + \delta_{charge}^2},\qquad(2)$$

where $\delta_{trigger}$=1.1%, δ_{track}=2.9%, and δ_{charge}=0.5% denote the corresponding systematic uncertainties of the trigger, track selection, and charge selection efficiencies, respectively. Systematic uncertainties corresponding to other very loose selections are negligible, where the total uncertainty is 3.1%.

With systematic uncertainties considered, the flux upper limit of $\frac{2}{3}e$ FCP is found to be $\Phi < 6.2 \times 10^{-10}$ cm^{-2}sr^{-1}s^{-1} [20].
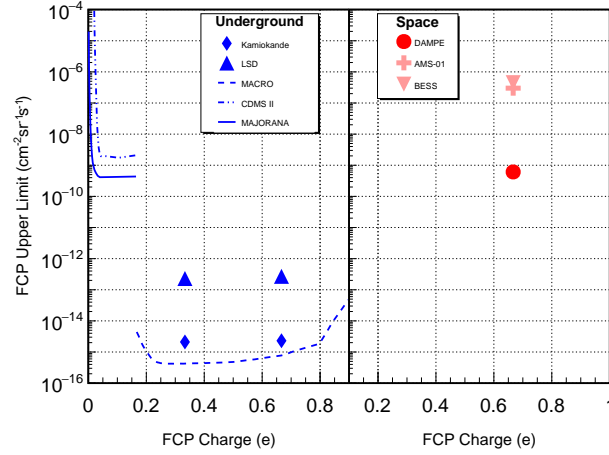
Figure 6: FCP flux upper limit versus electric charge from different cosmic ray experiments [20]. The results of underground experiments which require the particles to have energy above ∼ 100s GeV are shown in the left panel. The results of space experiments which detect the particles above a few GeV due to the limitation of geomagnetic cutoff are shown in the right panel. The DAMPE upper limit (red dot) is lower than those from AMS-01 [11] (light red cross) and BESS [12] (red inverted triangle). The results of the underground experiments such as LSD [6] (blue triangles), Kamiokande II [5] (blue full diamond), MACRO [7] (blue dashed line), CDMS II [9] (blue dotted line), and MAJORANA [10] (blue solid line) are shown also.

Table 2: The comparison between DAMPE and other similar types experiments [20].

Experiments	Geometric acceptance(cm^2sr)	Exposure time (s)	Upper limit ($cm^{-2}sr^{-1}s^{-1}$)
AMS-01	3000	3.6×10^4	3.0×10^{-7} (95% C. L.)
BESS	1500	3.2×10^5	4.5×10^{-7} (90% C. L.)
DAMPE	3000	2.3×10^7	6.2×10^{-10} (90% C. L.)

Table 2 presents the complete results and some vital parameters of DAMPE, compared with other similar experiments. Figure 6 shows the upper limits from other FCP searches. Among underground experiments, MACRO yields the most sensitive upper limit. The CDMS II and MAJORANA experiments have high degrees of sensitivity to small charges because of the lower thresholds of the respective detection systems. Among space equipment, AMS-01 has a large geometric acceptance [25], but a short exposure duration. BESS integrates data gathered over four flights to achieve a longer exposure time but its geometric acceptance is limited. DAMPE has the longest and continuous exposure time as well as relatively large geometric acceptance, and therefore it yields the most stringent FCP flux upper limit for space experiments, with an improvement of three orders of magnitude over previous work.

5. Summary

Based on on-orbit data obtained from DAMPE over a period of five years the results of the search for $\frac{2}{3}e$ FCPs in primary cosmic rays are as follows. No FCP signals are observed and a flux

upper limit of $\Phi < 6.2 \times 10^{-10}$ cm^{-2}sr^{-1}s^{-1} is established at the 90% C. L. A precise measurement of the flux or a conservative flux upper limit is essential to construct and constrain the model of FCPs. Most of the previously performed underground experiments assumed that FCPs would exhibit long penetration paths, which, in turn, requires them to have energy exceeding a few hundred GeV. Given the effective energy threshold arising from the geometric cutoff, experiments in space can be used to detect FCPs with energy as low as a few GeV. DAMPE serves as a novel observation platform and enables a long-term, continuous search for relatively low-energy FCPs in primary cosmic rays. In the future, with the accumulation of more on-orbit data, DAMPE is expected to perform even more sensitive FCP searches.

References

[1] R. A Millikan. *Phys. Rev.*, 29(6):560–561, 1909.

[2] M Gell-Mann. *Phys. Lett.*, 8(3):214–215, 1964.

[3] George Zweig. Technical report, CM-P00042884, 1964.

[4] M. L Perl et al. *Mod. Phys. Lett.*, 19(35):2595–2610, 2004.

[5] M Mori et al. *Phys. Rev. D.*, 43(9):2843, 1991.

[6] M Aglietta et al. *Astropart. Phys.*, 2(1):29–34, 1994.

[7] M Ambrosio et al. *Phys. Rev. D.*, 62(5):052003, 2000.

[8] M Ambrosio et al. *arXiv preprint hep-ex/0402006*, 2004.

[9] R Agnese et al. *Phys. Rev. Lett.*, 114(11):111302, 2015.

[10] S. I Alvis et al. *Phys. Rev. Lett.*, 120(21):211804, 2018.

[11] C Sbarra et al. *arXiv preprint astro-ph/0304192*, 2003.

[12] H Fuke et al. *Adv. Sp. Res.*, 41(12):2050–2055, 2008.

[13] J Chang et al. *Astropart. Phys.*, 95:6–24, 2017.

[14] Y Yu et al. *Astropart. Phys.*, 94:1–10, 2017.

[15] P Azzarello et al. *Nucl. Instrum. Methods A.*, 831:378–384, 2016.

[16] Z Zhang et al. *Nucl. Instrum. Methods A.*, 836:98–104, 2016.

[17] Y Huang et al. *Res. Astron. Astrophys.*, 20(9):153, 2020.

[18] T Dong et al. *Astropart. Phys.*, 105:31–36, 2019.

[19] S Vitillo et al. In *Proc. Sci.*, volume 301, page 240, 2017.

[20] F Alemanno et al. *Physical Review D*, 106(6):063026, 2022.

[21] F Alemanno et al. *Phys. Rev. Lett.*, 126(20):201102, 2021.

[22] Y Zhang et al. *Res. Astron. Astrophys.*, 19(9):123, 2019.

[23] S Agostinelli et al. *Nucl. Instrum. Methods A.*, 506(3):250–303, 2003.

[24] G. J Feldman et al. *Phys. Rev. D.*, 57(7):3873, 1998.

[25] J Alcaraz et al. *Phy. Lett. B*, 461(4):387–396, 1999.